Author's Accepted Manuscript

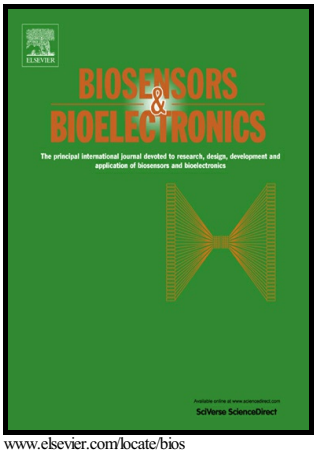

www.elsevier.com/locate/bios

CdZnTeS quantum dots based electrochemiluminescent image immunoanalysis

Xiu-Li Liang, Ning Bao, Xiliang Luo, Shou-Nian Ding

PII: S0956-5663(18)30428-7
DOI: https://doi.org/10.1016/j.bios.2018.06.006
Reference: BIOS10526

To appear in: *Biosensors and Bioelectronic*

Received date: 11 May 2018
Accepted date: 2 June 2018

Cite this article as: Xiu-Li Liang, Ning Bao, Xiliang Luo and Shou-Nian Ding, CdZnTeS quantum dots based electrochemiluminescent image immunoanalysis, *Biosensors and Bioelectronic,* https://doi.org/10.1016/j.bios.2018.06.006

CdZnTeS quantum dots based electrochemiluminescent image immunoanalysis

Xiu-Li Liang[a], Ning Bao[b], Xiliang Luo[c], Shou-Nian Ding[a*]

[a]*Jiangsu Province Hi-Tech Key Laboratory for Bio-medical Research, School of Chemistry and Chemical Engineering, Southeast University, Nanjing 211189, China.*

[b]*School of Public Health, Nantong University, 226019 Nantong, Jiangsu, China.*

[c]*Key Laboratory of Sensor Analysis of Tumor Marker, Ministry of Education, College of Chemistry and Molecular Engineering, Qingdao University of Science and Technology, Qingdao 266042, China.*

[*]Corresponding author. (S.-N. Ding) Fax: (+86) 25-52090621. snding@seu.edu.cn.

Abstract:

In this work, quaternary CdZnTeS quantum dots (QDs) with a particularly strong electrochemiluminescence (ECL) were synthesized as ECL signal labels. The strong ECL signals can be obtained at both cathode and anode with the ECL efficiencies of 19.78% and 1.62%, respectively. The sandwich-structured ECL immunosensors for the detection of alpha-fetoprotein (AFP) and cancer antigen 125 (CA125) were accomplished with direct ECL image analysis. Under optimal conditions, the QDs-based ECL image immunoanalysis possessed good linearity from 0.5 ng/mL to 20 ng/mL for AFP and from 20 U/mL to 500 U/mL for CA125 with the detection limit of 0.1 ng/mL and 6 U/mL, respectively (S/N=3), and the lower detection limit obtained by photomultiplier tube were 0.1 fg/mL for AFP and 0.03 mU/mL for CA125 with the wide dynamic range from 0.5 fg/mL to 20 ng/mL and from 0.1 mU/mL to 500 U/mL, respectively (S/N=3). Furthermore, the ECL immunoanalysis was evaluated with commercial enzyme-linked immunosorbent assay in human serum samples. The good results indicated that CdZnTeS QDs-based ECL biosensor has great potential for fast biomedical screening and multi-assays in clinical diagnosis.

Keywords: CdZnTeS QDs; Immunosensors; Electrochemiluminescent image analysis; Alpha-fetoprotein; Cancer antigen 125

1 Introduction

The unprecedented scientific research boom about quantum dots (QDs) has occurred over the past few decades, owing to their unique size/composition-dependent physical and chemical characteristics (Amelia et al. 2012; Ding et al. 2002). In this family of QDs, considerable attention has been paid to cadmium-based QDs including the homogeneous structures (CdTe, CdSe, CdS) (Han et al. 2017; Kalytchuk et al. 2016; Liu and Ding 2016), core-shell structures (CdTe/CdS) (Jing et al. 2015), and doped structures (Ding et al. 2015). Compared with above-mentioned QDs, quaternary alloy QDs had great potential in both academic research and commercial fields due to their optical and electronic properties, which can be adjusted by altering not only the particle size but also the composition of the alloyed QDs (Yang et al. 2013). Most importantly, multiple alloy QDs were endowed with a wider adjustable band gap and much higher photoluminescent quantum yield (Deng et al. 2013a; Deng et al. 2013b). As reported, electrogenerated chemiluminescence (ECL) is a light-emitting process via the excited state of luminophore, which is based on electrochemical stimulation (Bard 2004). To date, ECL behaviours of QDs have been reported extensively, but the ECL signal of most unmodified QDs was usually lower than that of $Ru(bpy)_3^{2+}$ or luminal systems, which limited the applications of QDs ECL in biological immunoassays. Therefore, the development of novel QDs with extremely high ECL intensity has promising potential for bioassays.

Biomarker was regarded as an indicator of cancer existence in human body, and the detection of biomarkers can provide useful information for early cancer diagnosis and effective monitoring therapeutic effects, which significantly improved the performance of routine cancer diagnostics. Up to now, several immunoassays for detection of biomarkers were currently available, such as colorimetric immunoassay

(Burke et al. 2016), fluorescence immunoassay (Li et al. 2014), electrochemistry immunoassay (Chikkaveeraiah et al. 2012), ECL immunoassay (Huang et al. 2015) and so on. Over other analytical methods, the ECL technique has gained increasing attention due to their inherent advantages such as fast response, high sensitivity and easy operation (Hu and Xu 2010; Zhao et al. 2015a). Particularly, ECL imaging technology can further enhance the analytical capabilities. However, the reports about ECL imaging were limited. In recent publications, ECL imaging and bipolar electrode system were combined to detect cancer biomarkers (Wu et al. 2015; Wu et al. 2013). Liu et al. developed an open bipolar electrode-ECL sensing for visual detection of H_2O_2 and TPA (Liu et al. 2015). Zhou and colleagues measured active membrane cholesterol at single living cells by ECL imaging (Zhou et al. 2015). Obviously, ECL imaging was mainly obtained by using the traditional $Ru(bpy)_3^{2+}$/co-reactant system and luminol/hydrogen peroxide system. Therefore, it is of great significance to develop novel ECL nanomaterial to replace traditional luminophore for ECL imaging immunoassays.

In theory, the reaction system suitable for ECL can be used for ECL imaging immunoassays. However, considering the luminescent efficiency and the stability of luminescent system, two aspects should be considered. On one hand, a suitable carrier to immobilize the biomolecules is a major factor in the biosensor design. Different kinds of carriers including bionanospheres (Du et al. 2010), colloidal gold nanoparticles (Lai et al. 2013), graphene oxide (Feng et al. 2016), and magnetic beads (Ren et al. 2017; Tang et al. 2013) have been used to load biomolecules. More recently, Fe_3O_4 nanoparticles (NPs) became more attractive due to their many excellent features. For instance, large specific surface area allowed to increase totals of loaded biomolecules; Fast and simple separation could be achieved with the help of an external magnet to eliminate nonspecific adsorption. In addition, the biocompatibility and super-paramagnetic nature of Fe_3O_4 NPs was also the prerequisites for their suitability in a variety of biological applications, for example, bio-separation (Tang et al. 2013), drug delivery (Sahoo et al. 2013) and as carrier for antibody (Sung et al. 2013). On the other hand, label with high luminescent efficiency

is the basic element for capturing the visible ECL imaging by cell phone. In fact, numerous substances associated with ECL such as QDs (Xu et al. 2017), $Ru(bpy)_3^{2+}$ (Li et al. 2017), and luminol (Jiang et al. 2014) have been used as the labels for sandwich immunosensor. However, $Ru(bpy)_3^{2+}$ should be functionalized with other groups to be utilized in immunoanalysis, and the functional procedure was cumbersome and harsh (Zhou et al. 2014). As for luminol, whose ECL signal is very strong in alkaline condition, but very weak in neutral solution, which restricted its application in the biological analysis fields (Qi and Zhang 2004). In contrast, QDs had several advantages including facile preparation, easy modification, size-dependent wavelength and simple conjugation with biomolecules (Wu et al. 2014; Yao et al. 2017), to play a role as ECL labels. It is also a new breakthrough for QDs to be used in ECL image immunoassay.

In this work, quaternary CdZnTeS QDs were synthesized, and the ECL behaviors have been investigated carefully. The results demonstrated that the strong ECL signals of CdZnTeS QDs can be detected both at cathode and anode (Scheme 1A). The calculated ECL efficiencies were 19.78% and 1.62%, respectively. In addition, a visualized immunosensor (Scheme 1B) based on CdZnTeS QDs was proposed for the determination of alpha-fetoprotein (AFP) and cancer antigen 125 (CA125). The sandwich-type immunosensor was developed by utilizing Fe_3O_4@SiO_2-Ab_1 nanocomposites as the magnetically sensor platform and CdZnTeS QDs-Ab_2 as the signal probe. For ECL measurement, $K_2S_2O_8$ was employed as co-reactants, and the ECL image can be taken by a cell phone. By means of analyzing the image via Image-Pro Plus, quantitative analysis could be realized. In a certain concentration ranges of AFP and CA125, the ECL signal increased linearly with the increasing concentration. The satisfactory results indicated that the resulting bioimaging platform can be a powerful tool for the detection of various kinds of biomarkers in real-sample analysis.

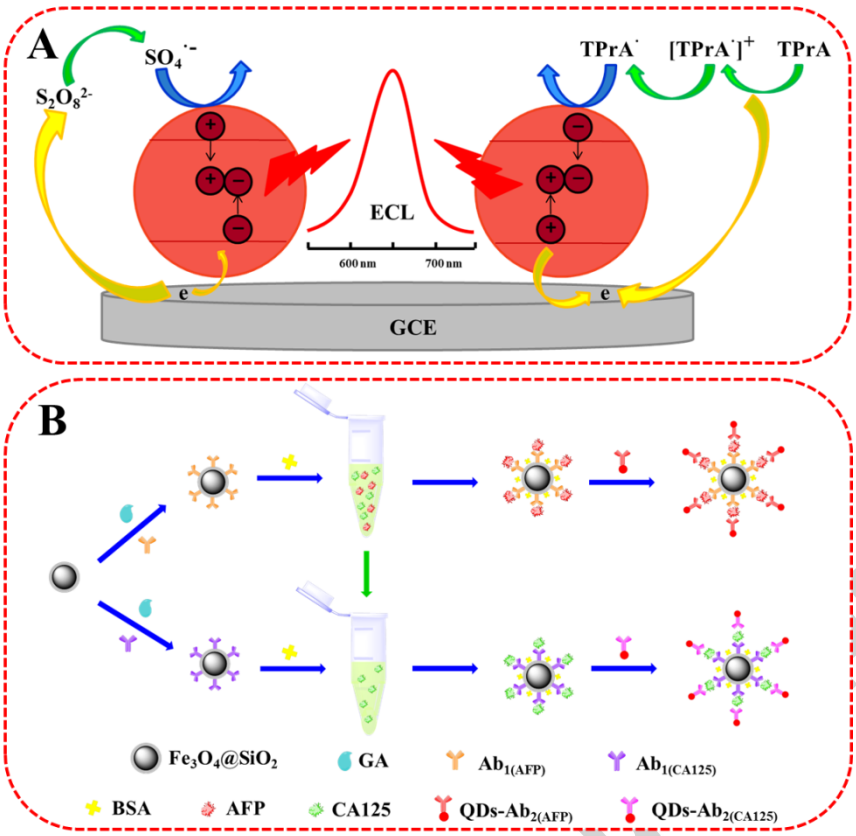

Scheme 1. Schematic illustrations of (A) ECL mechanism of CdZnTeS QDs and (B) the fabrication process of proposed ECL immunosensor.

2 Experimental section

2.1 Reagents and chemicals

AFP antigen (AFP), anti-AFP antibody ($Ab_{1(AFP)}$, $Ab_{2(AFP)}$), CA125 antigen (CA125) and anti-CA125 antibody ($Ab_{1(CA125)}$, $Ab_{2(CA125)}$) were purchased from Linc-Bio Science Co., Ltd (Shanghai, China). All other reagents were shown in supporting information (SI).

2.2 Apparatus and measurements

All electrochemical experiments for ECL were measured on a MPI-M Analyzer (Xi'an Remax Analysis Instrument Co., Ltd, Xi'an, China). The ECL images were photographed by a Huawei mobile phone, and the pictures were analyzed by Image-Pro Plus, detailed analysis method was shown in section 2.7. And other instruments were shown in the SI.

2.3 Synthesis of CdZnTeS QDs

CdZnTeS QDs were synthesized according to literature (Adegoke and Park 2016)

with some modification. Detailed synthesis steps were displayed in SI. In this paper, CdZnTeS1~CdZnTeS5 represent different sizes of CdZnTeS QDs.

2.4 Preparation of CdZnTeS5-Ab_2 probe

QDs-Ab_2 conjugates were prepared according to our previous work (Zhang and Ding 2016). Taking CdZnTeS5-$Ab_{2(AFP)}$ as an example, first, 75 μL of freshly prepared EDC solution (4.2 mg/mL) was added into 50 μL of CdZnTeS5 QDs (6 mg/mL, which was obtained at 6 h under 110 °C reflux) to activate the carboxylic acid groups on QDs surface. Then, 1 mL of $Ab_{2(AFP)}$ (10 μg/mL) was added into above solution, and allowed to react for 2 h at room temperature (RT) with gentle shaking in dark. At last, the obtained product was ultrafiltrated by using 50 KD filter (*3,000 g* for 10 min) to remove unconjugated QDs and byproduct. The resultant mixture was stored at 4 °C until use.

2.5 Preparation of Fe_3O_4@SiO_2-Ab_1

Fe_3O_4 NPs were prepared using a hydrothermal method according to a previously reported literature (Liu et al. 2009). Fe_3O_4@SiO_2 core/shell colloids were prepared through a Stöber process (Ge and Yin 2008), and the amination procedure was carried out according to previous method without change (Li et al. 2015a).

$Ab_{1(AFP)}$ were assembled to the aminated Fe_3O_4@SiO_2 through cross-linking reaction with glutaraldehyde (GA). Briefly, 10 mg of aminated Fe_3O_4@SiO_2 was dissolved in 7.5 mL ultra-pure water thoroughly, and then 2.5 mL of GA solution (2.5 wt%) was added into the above solution and stirred at RT for 6 h. The mixture was washed several times with 10 mM PBS (pH 7.4) by magnetic separation to remove the excess GA. The obtained product was redispersed in 5 mL of PBS (10 mM, pH 7.4). Subsequently, 500 μL of solution containing 10 μg/mL $Ab_{1(AFP)}$ was added into 500 μL GA-functionalized Fe_3O_4@SiO_2, the mixture was allowed to react for 1 h under soft shaking at RT (Xing et al. 2007; Zhao et al. 2015b), and then washed with 10 mM PBS (pH 7.4) to clear away unconjugated $Ab_{1(AFP)}$. Finally, the $Ab_{1(AFP)}$-conjugated Fe_3O_4@SiO_2 was incubated in PBS solution containing BSA (100 μL, 1.0 wt%) to block the nonspecific binding sites. The obtained Fe_3O_4@SiO_2/$Ab_{1(AFP)}$/BSA bioconjugates were redispersed in 500 μL PBS after washing, and stored at 4 °C for next

step. Fe_3O_4@SiO_2-$Ab_{1(CA125)}$ was prepared by the similar procedures, except that $Ab_{1(AFP)}$ was replaced by $Ab_{1(CA125)}$.

2.6 Fabrication of the immunosensor

The fabrication process of the immunosensor was displayed in Scheme 1B. Fe_3O_4@SiO_2-$Ab_{1(AFP)}$ solution (50 μL) was added into solution A (5 mL PBS solution containing different concentration of antigens), and shaked at 37 °C for 1 h. The obtained antigen-antibody complex was washed with PBS carefully to remove physically adsorbed antigen. Then, CdZnTeS5-$Ab_{2(AFP)}$ was mixed with the above solution and incubated for 1 h to fabricate sandwich-type immunosensor. Finally, the resulting immunosensor was washed with PBS to remove unbound CdZnTeS5-$Ab_{2(AFP)}$, then redispersed in 100 μL PBS solution and stored at 4 °C for future use. For the construction of CA125 immunosensor, 50 μL of the Fe_3O_4@SiO_2-$Ab_{1(CA125)}$ was put into the remaining solution A, the following steps were similar to AFP biosensor.

2.7 The procedure of ECL measurement and data analysis

The ECL measurement of CdZnTeS QDs was carried out via a traditional three-electrode system. $K_2S_2O_8$ and TPrA were selected as co-reactants for cathodic ECL and anodic ECL, respectively. For the ECL detection of AFP and CA125, 10 μL of the above immunosensors with various concentrations of AFP and CA125 was dropped on GCE and dried in air at RT. Four milliliters of 0.1 M PBS solution (pH 7.4) containing 50 mM $K_2S_2O_8$ was added into the detector cell. In the detection process, photomultiplier tube (PMT) was set at 450 V, the applied potential was 0~ -1.6 V, the scan rate was 100 mV s^{-1}.

Moreover, the visual ECL images were collected by cell phone under the above mentioned condition. The resulting images were analyzed by Image-Pro Plus, which converts the brightness of each pixel on the picture to photon counts. The ECL intensity was calculated by integrating the photon count for each pixel of the ECL-active area of the picture.

3 Results and discussion

3.1 Characterizations of CdZnTeS QDs

Typical TEM (Figure S1A) was used to characterize the morphology and size of

CdZnTeS5 QDs. It can be observed that CdZnTeS5 QDs were nearly spherical particles with the average diameter of 6.79 nm. As shown in Figure S1B, powder XRD pattern for CdZnTeS5 QDs depicted a consistent single crystalline domain feature, which exhibited a zinc-blend crystal structure with planes at {111}, {220} and {311} (Adegoke and Park 2016). In Figure S1C and S1D, UV absorption peaks and fluorescence emission peaks of CdZnTeS QDs presented red-shift with the size of QDs increases. As depicted in Figure S2, EDX analysis of CdZnTeS5 QDs demonstrated the presence of Cd, Zn, Te and S elements, and further confirmed the formation of CdZnTeS quaternary-alloyed QDs.

3.2 ECL behavior of CdZnTeS QDs

Figure 1A and 1B showed the ECL behaviors of CdZnTeS QDs in 0.1 M PBS solution (pH 7.4) containing 10 mM $K_2S_2O_8$ (PMT: 300 V) and 10 mM TPrA (PMT: 350 V), respectively. The ECL intensities of CdZnTeS QDs increased with the increasing of particle size both at cathode and anode because of the size effect (Liu et al. 2007). The CV curves of modified GCE in 0.1 M PBS (pH 7.4) containing 10 mM $K_2S_2O_8$ and 10 mM TPrA were showed in Figure S3. As reported, ECL is generated by relaxation of excited-state molecules, which are produced through electron-transfer annihilation of electrogenerated anion and cation radicals (Ding et al. 2002). In the potential region for CdZnTeS QDs reduction, electrons are injected into the CdZnTeS nanocrystals and the anion radicals（$CdZnTeS^{\cdot-}$） are formed. Simultaneously, $S_2O_8^{2-}$, as co-reactant, produces strong oxidant, $SO_4^{\cdot-}$, and then $SO_4^{\cdot-}$ can react with $CdZnTeS^{\cdot-}$ by injecting a hole into the highest occupied molecular orbital to produce an excited state of the QDs. The ECL mechanism can be drawn as follows:

$$CdZnTeS + e^- \rightarrow CdZnTeS^{\cdot-} \quad (1)$$

$$S_2O_8^{2-} + e^- \rightarrow SO_4^{2-} + SO_4^{\cdot-} \quad (2)$$

$$CdZnTeS^{\cdot-} + SO_4^{\cdot-} \rightarrow CdZnTeS^* + SO_4^{2-} \quad (3)$$

$$CdZnTeS^* \rightarrow CdZnTeS + h\nu \quad (4)$$

TPrA was another important co-reactant for ECL systems. The whole process for the TPrA involved in the ECL of CdZnTeS QDs can be deduced as equation (5) ~ (8). Upon oxidation, the short-lived TPrA radical cation ($TPrA^{\cdot+}$) lose a proton from an

α-carbon to form the strongly reducing intermediate ($TPrA^{\cdot}$). At last, the electrogenerated oxidized CdZnTeS QDs ($CdZnTeS^{\cdot+}$) react with $TPrA^{\cdot}$ to produce the ECL emission (Omer and Bard 2009).

$$CdZnTeS - e^{-} \rightarrow CdZnTeS^{\cdot+} \quad (5)$$

$$TPrA - e^{-} \rightarrow TPrA^{\cdot+} \rightarrow TPrA^{\cdot} + H^{+} \quad (6)$$

$$CdZnTeS^{\cdot+} + TPrA^{\cdot} \rightarrow CdZnTeS^{*} + TPrA \quad (7)$$

$$CdZnTeS^{*} \rightarrow CdZnTeS + h\nu \quad (8)$$

It is believed that ECL spectrum represented surface state transitions and FL spectrum mainly reflected the band gap of QDs. Highly-passivated QDs without deep surface trap state showed an overlap in the ECL and FL spectra, owing to the band gap engineered model of ECL (Liu et al. 2014; Myung et al. 2003). In Figure 1C and 1D, the main peak of CdZnTeS5 QDs for the ECL spectrum coincided with the emission peak position of the FL spectrum, indicating that the surfaces have been largely passivated. According to the previous reports (Bell and Sen 1985; Li et al. 2010), the passivated surface state resulted from the formation of Zn-Te bond after zinc was fused into CdTe nanostructures. Unfortunately, the ECL spectra of other four kinds of QDs could not be obtained by PG2000-pro scientific class spectrometer, because their ECL intensities were relatively low. Herein, the ECL spectra obtained by employing several band-pass filters between the PMT and modified GCE (Lee et al. 2004) were displayed in Figure S4. Obviously, the wavelength of maximum emission for the ECL spectrum was very close to that of the corresponding FL spectrum, which also manifested that the ECL emission of QDs presented red-shift with the size of QDs increases.

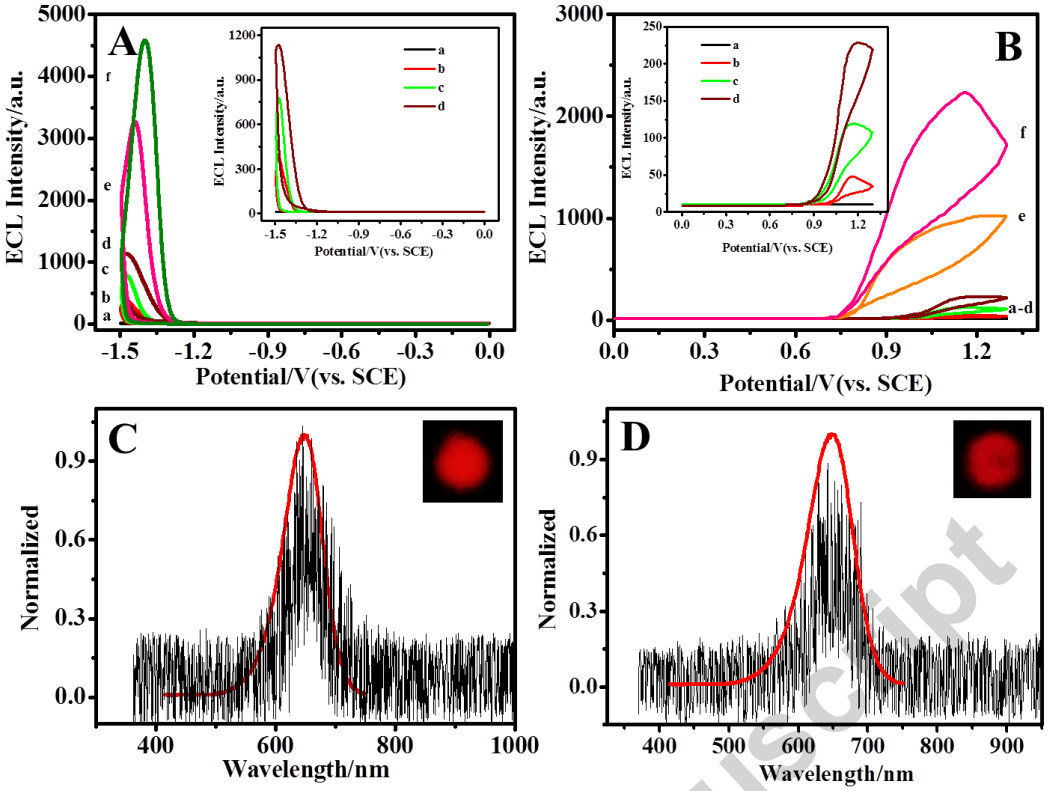

Fig 1. ECL-potential curves of CdZnTeS QDs modified GCE in 0.1 M PBS (pH 7.4) containing (A) 10 mM $K_2S_2O_8$ and (B) 10 mM TPrA (a: bare GCE, b-f: CdZnTeS1-CdZnTeS5 modified GCE). Comparison of solid-state FL spectrum (red line) and ECL spectrum (black line) of CdZnTeS5 QDs detected in 0.1 M PBS (pH 7.4) containing (C) 10 mM $K_2S_2O_8$ and (D) 10 mM TPrA, respectively (The inset are ECL photos).

The ECL efficiency was defined as the number of photons per electron transferred during the chemiluminescent reaction. It is the result of the efficiency of excited state and the quantum yield of emission from that excited state, which can be calculated by using the following equation (Ouyang et al. 1989; Wang et al. 2010):

$$\emptyset x = \emptyset st \left(\frac{\int_0^t Idt}{\int_0^t idt}\right)_x \Big/ \left(\frac{\int_0^t Idt}{\int_0^t idt}\right)_{st}$$

Here, $\emptyset_{st}$ was the ECL quantum efficiencies of $[Ru(bpy)_3]^{2+}$ (1 mM and 0.1 M (TBA)PF_6/acetonitrile) via annihilation, taken as 5.0% (Wallace and Bard 1979). $[Ru(bpy)_3]^{2+}$ was used as a relative standard, *x* represented the sample. *I* was ECL intensity, *i* was current value. The calculated ECL efficiency of the CdZnTeS5 QDs

was 19.78% for cathode and 1.62% for anode. To the best of our knowledge, this is the highest efficiency obtained for unmodified QDs.

We also studied the effect of cadmium-to-zinc molar ratio on the ECL intensity of CdZnTeS QDs. The results (Figure S5A) showed that 10: 0.5 was the optimum molar ratio of cadmium-to-zinc. Thus, the following experiments were all conducted at a ratio of 10:0.5. Figure S5B depicted the ECL transients of CdZnTeS5 QDs by stepping the potential between +1.3 V and -1.5 V in 0.1 M PBS solution (pH 7.4), the results further demonstrated that CdZnTeS QDs can generate light both at cathode and anode. In addition, the cathodic ECL signal of CdZnTeS5 QDs was obviously higher than its anodic ECL signal. Thus, quantitative analysis of AFP and CA125 were detected at cathode.

3.3 Characterization of QDs-Ab_2 probe.

The AFP biosensor was selected as an example to characterize the construction process because the CA 125 immunosensor was constructed by the identical method. Agarose gels electrophoresis experiment was carried out to demonstrate the conjugation of QDs with Ab_2. A mixture of sample (13 μL) and glycerol (2 μL) were run on a 0.8% agarose gel at 100 V in the TAE buffer solution. As the results shown in Figure 2A, compared with pure QDs and QDs activated by EDC, QDs-Ab_2 conjugates ran quite slow, for that the larger size of QDs-Ab_2 conjugates. Therefore, the results of gel electrophoresis declared that QDs and Ab_2 were successfully linked.

3.4 Characterization of Fe_3O_4@SiO_2/Ab_1

We compared the effects of different magnetic beads (The synthesis process was similar to literature (Dong et al. 2017; Zhang and Ding 2017) on the detection of AFP antigen. By comparing the ECL intensities, Fe_3O_4@SiO_2 was chosen as nano-carriers for immunoassay (Figure S6, Table S1), which can also be evidenced by confocal fluorescence imaging, as shown in Figure 2C-E. TEM image of the synthesized Fe_3O_4@SiO_2 was employed (Figure 2B) to characterize the size and morphology. It can be observed that the prepared Fe_3O_4@SiO_2 possessed uniform size and well-dispersion with an average diameter of 310 nm (core 190 nm, shell 60 nm). In addition, amino modification on the surface of Fe_3O_4@SiO_2 NPs was confirmed by

FT-IR spectrum (Figure S7), the analysis of results was shown in SI. To prove that Ab_1 has been attached to $Fe_3O_4@SiO_2$, FITC-labeled $Ab_{1(AFP)}$ was used to connect with magnetic NPs, the conjugates produce green fluorescence under blue light excitation can be observed clearly in Figure 2C-E, which were recorded with confocal microscopy. The results further indicated that Ab_1 have been attached to the magnetic NPs.

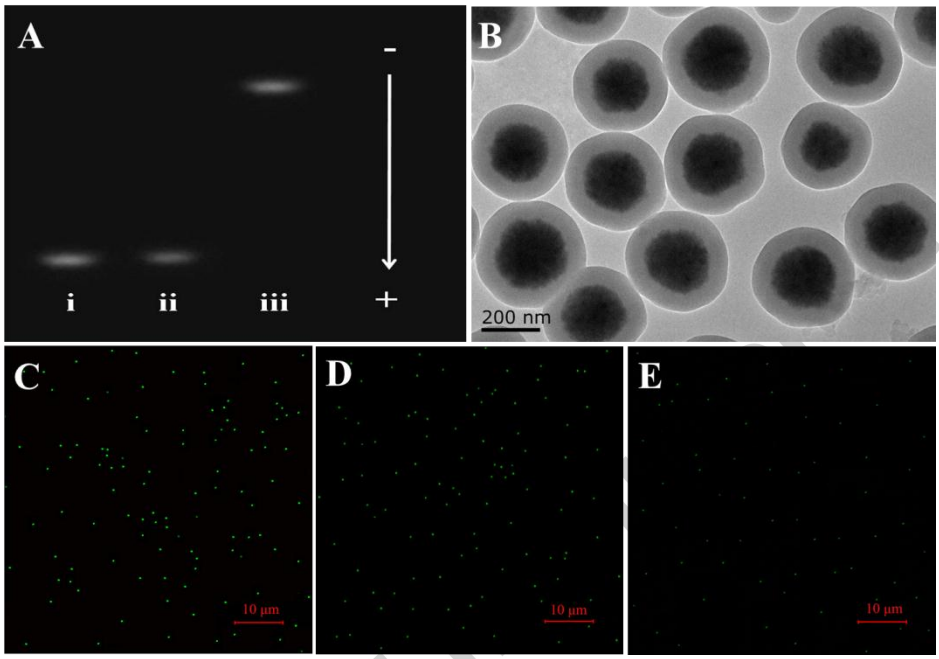

Fig 2. (A) Agarose gel electrophoresis image of the QDs (i), QDs activated by EDC (ii) and QDs-Ab_2 conjugates (iii); (B) TEM image of the $Fe_3O_4@SiO_2$ NPs; Confocal fluorescence images of (C) $Fe_3O_4@SiO_2$/FITC labeled-$Ab_{1(AFP)}$, (D) $Fe_3O_4@SiO_2$@PS/FITC labeled-$Ab_{1(AFP)}$ and (E) Fe_3O_4@Au/FITC labeled-$Ab_{1(AFP)}$.

3.5 EIS monitoring of the immunosensor fabrication process

Electrochemical impedance spectroscopy (EIS) was employed to probe the interfacial properties of modified electrodes. It is well known that the semicircle diameter in EIS equals to the electron transfer resistance (R_{et}) and the linear area at lower frequencies represents the diffusion process (Li et al. 2015b). EIS of each step of the immunosensor construction and the Randle's equivalent circuit were shown in Figure S8. It could be found that the R_{et} value of the bare GCE was almost a straight line (curve a), meaning that the bare electrode has good conductivity. For $Fe_3O_4@SiO_2/Ab_{1(AFP)}$ modified electrode, the EIS exhibited an increased R_{et} value

(R_{et}=741.4 Ω, curve b) due to Fe_3O_4@SiO_2/$Ab_{1(AFP)}$ layer obstructed the movement of the $[Fe(CN)_6]^{3-/4-}$ redox probe to the electrode surface. After Fe_3O_4@SiO_2/$Ab_{1(AFP)}$ was blocked by BSA, the value of R_{et} increased markedly (R_{et}=1069 Ω, curve c) for that BSA further hindered the diffusion process. Similarly, the R_{et} value were continued to increase after incubated in AFP antigen (R_{et}=2756 Ω, curve d) and CdZnTeS5-$Ab_{2(AFP)}$ (R_{et}=4801 Ω, curve e), which were ascribed to the fact that the introduced proteins and formed immune complexes act as the blocking layers to hinder the electron transfer. EIS results certified that the immunosensor was fabricated successfully.

3.6 Analytical performance of the multiplexed immunoassay

Prior to experiment, the parameters including the incubation time (Figure S9), the amount of GA-functionalized Fe_3O_4@SiO_2, pH of PBS for antigen-antibody immunoreaction and the amount of QDs added during labeling process were optimized (Figure S10). The ECL assay of the fabricated immunosensor was carried out under the optimized conditions. Figure 5A and 5B displayed a series of visualized ECL images of the immunosensor for different concentrations of AFP and CA125. The ECL emission of the immunosensor turned weaker as the concentrations of antigen decreased from 20 ng/mL to 0.5 ng/mL for AFP and from 500 U/mL to 20 U/mL for CA125. The intensity of the visible ECL can be analyzed by the free software called Image-Pro Plus through calculating the area and the lightness of the ECL image, which was conducted in accordance with previous literatures (Chang et al. 2012; Liu et al. 2015). As revealed in Figure 5C and 5D, the intensities in the ECL images were proportional to lgC_{AFP} and lgC_{CA125}. The linear fitting regression equations could be expressed as $I=22.07lgC_{AFP}+21.71$ with a correlation coefficient of 0.9875 for AFP and $I=24.23lgC_{CA125}-16.58$ with a correlation coefficient of 0.99 for CA125. The ECL images of the biosensors with relatively low concentrations of antigen can be photographed by a mobile phone, which demonstrated that an ultra-sensitive immunosensor was constructed and the developed approach has the great potential for the practical applications.

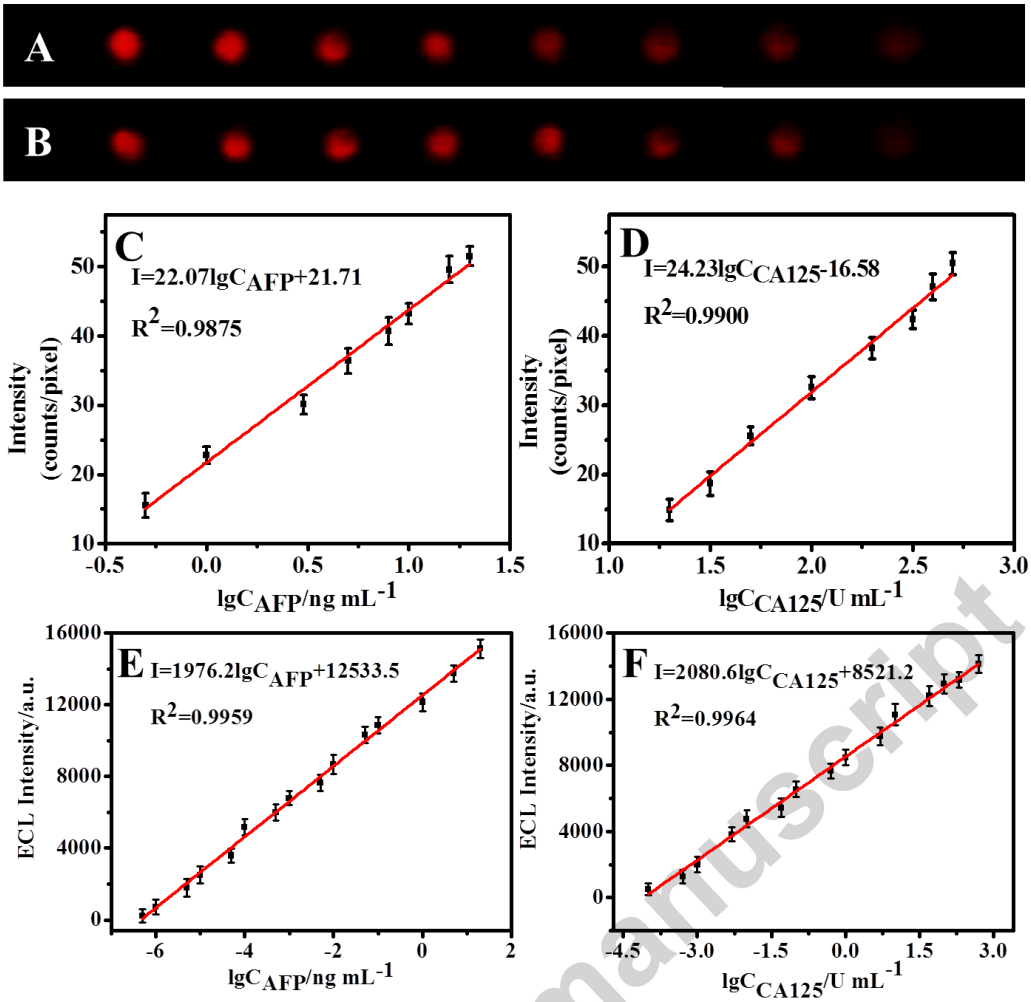

Fig 3. Visualized ECL images of AFP (A) and CA125 (B) immunosensor photographed by cell phone. From left to right, the concentrations of AFP are 20, 15, 10, 8, 5, 3, 1, 0.5 ng/mL, and the concentrations of CA125 are 500, 400, 300, 200, 100, 50, 30 and 20 U/mL, respectively. The linear relationship between the light intensity in the ECL images vs. (C) lgC_{AFP} and (D) lgC_{CA125}. Error bars were obtained from three experiments. ECL linear relationship of (E) AFP (0.5, 1, 5, 10, 50 fg/mL; 0.1, 0.5, 1, 5, 10, 50 pg/mL; 0.1, 1, 5, 20 ng/mL) and (F) CA125 (0.1, 0.5, 1, 5, 10, 50 mU/mL; 0.1, 0.5, 1, 5, 10, 50 , 100, 200, 500 U/mL) immunosensor detected in 0.1 M PBS (pH 7.4) containing 50 mM $K_2S_2O_8$ via PMT.

Under the optimized experimental condition, ECL measurements by PMT were carried out to quantitatively detect AFP and CA125. As revealed in Figure 3E and 3F, the ECL intensities for AFP and CA125 increased with an increasing in the concentrations of AFP and CA125. The peak intensities of AFP and CA125 were proportional to the logarithmic concentrations of AFP and CA125 individually. The

linear correlation coefficients were 0.9959 for AFP and 0.9964 for CA125. The detection limit was 0.1 fg/mL for AFP and 0.03 mU/mL for CA125 at a signal-to-noise ratio of 3. The comparison of the working ranges and detection limits between the proposed immunosensor and some other determination methods were listed in Table S2. It is obvious that our method presented a lower detection limit with wider linear range.

3.7 Evaluation of stability, reproducibility and specificity for immunoassays

The stability of the constructed immunosensor was tested by checking ECL response periodically (Figure 4A and 4B). The ECL intensity retained 91% of its initial value after stored at 4 °C for a week, suggesting that the stability of immunosensor was excellent. The reproducibility (Figure 4C and 4D) of the as-fabricated immunosensor was investigated by detecting AFP (0.5 ng/mL) and CA125 (30 U/mL), the relative standard deviation (RSD) were 1.27% for AFP and 2.35% for CA125, respectively. The low RSD indicated that the immunosensor could be used repeatedly. Additionally, to study the specificity of the immunosensor, interfering substances including 10 ng/mL of BSA, glucose (Glu), human immunoglobulin G (IgG) and uricacid (UA) were added into AFP (0.5 ng/mL) and CA125 (30 U/mL) antigen to construct immunosensor. Figure 4E and 4F showed ECL responses of pure AFP and CA125, and that obtained from AFP and CA125 containing an interferential substance. The RSD value of AFP for the mixture detection was 3.69%, and that of CA125 was 2.35%. The result indicated that the specificity of the immunosensor was satisfactory.

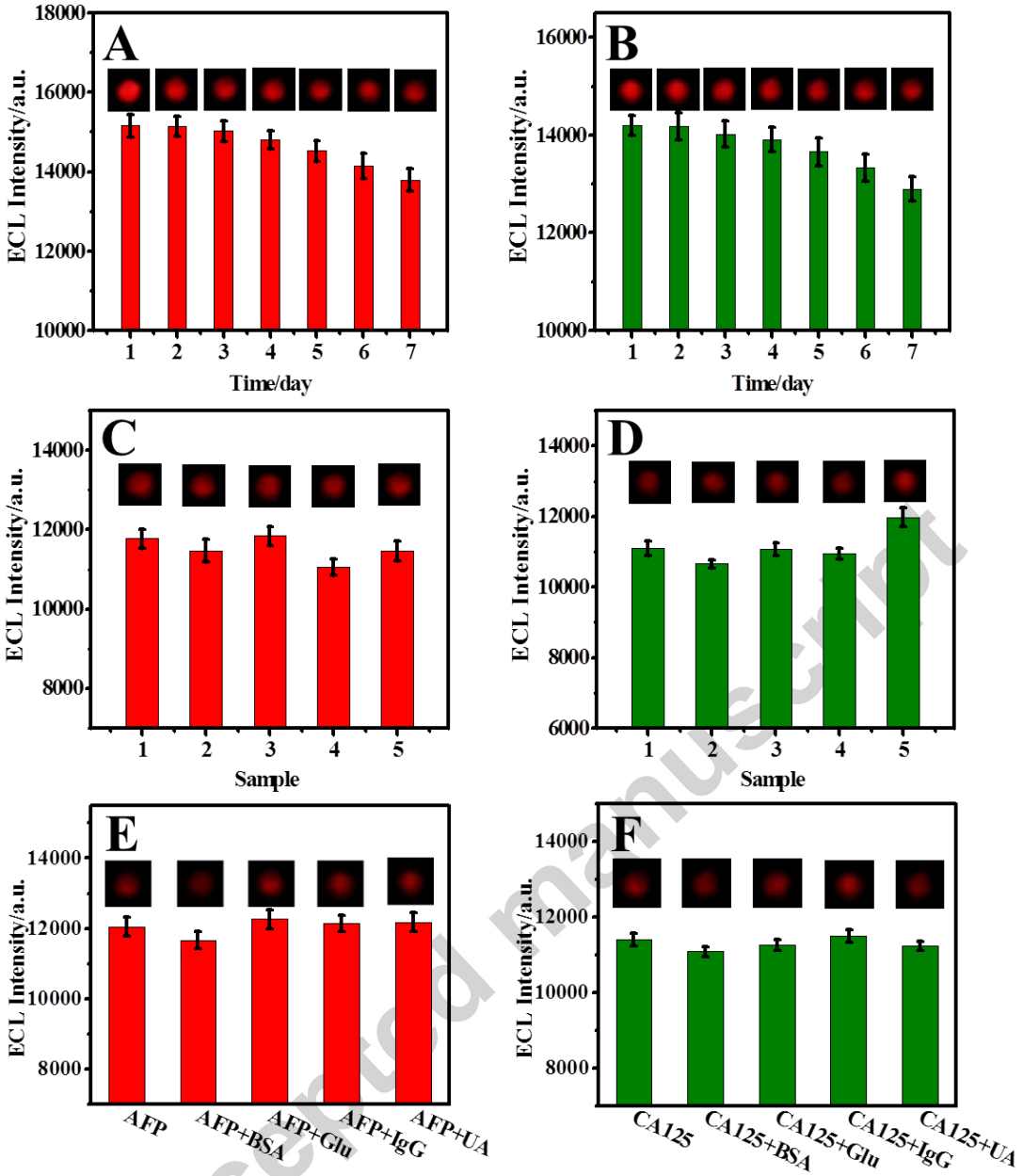

Fig 4. Stability (A, B), reproducibility (C, D) and specificity (E, F) of AFP immunosensor (left column) and CA125 immunosensor (right column). Insets are the corresponding ECL images.

3.8 Real sample analysis

To investigate the analytical performance and application potential of the proposed immunosensor, human serum samples obtained from Nanjing Zhongda Hospital were used for assay. As shown in Table 1, enzyme-linked immunosorbent assay (ELISA) was used as a reference. The measured values by proposed

immunosensor were consistent with the results by ELISA, indicating good accuracy of the proposed method for the determination of AFP and CA125. Recovery tests were carried out to verify the reliability of the developed immunosensor using the standard addition method (Table S3), and results revealed that the recovery ranged from 96.76% to 104.69%, and RSD ranged from 1.51% to 3.38%. The results manifested that the proposed immunoassay provided a potential application of clinical screening for early-stage cancers.

Table 1. Detection of AFP and CA125 in the serum samples using the proposed immunosensor and commercial ELISA method.

Sample	Commercial ELISA method	Our method	ECL image	Relative derivation (%)
AFP	4.18 ng/mL	4.06 ng/mL		-2.87
	3.22 ng/mL	3.41 ng/mL		5.90
	1.89 ng/mL	1.92 ng/mL		1.59
CA125	27.50 U/mL	28.68 U/mL		4.29
	24.75 U/mL	23.01 U/mL		-7.03
	20.06 U/mL	21.22 U/mL		5.78

Conclusions

In summary, water-soluble CdZnTeS QDs with strong ECL were synthesized, and the ECL behaviors at the cathode and anode were studied in detail, results have shown that the ECL efficiency of CdZnTeS QDs was particularly high. Based on the strong ECL performance of CdZnTeS QDs, a visual and efficient immunosensor technique for the detection of AFP and CA125 was presented. In this process, Fe_3O_4@SiO_2 magnetic NPs were selected as carriers for loading large amounts of antibody for signal amplifying and simplifying the procedures. On the other hand, quaternary CdZnTeS nanocrystals with ultra-strong ECL were chosen as labels to improve the sensitivity. As a low-cost tool for the determination of tumor markers, this immunoassay showed excellent performance for biomarkers detection, which might become a powerful tool for the determination of other protein target, and open a new avenue to clinical analysis. Unfortunately, the visualization of other four kinds of CdZnTeS QDs cannot be recorded at present, because their ECL intensities were

relatively low. In future work, the new synthetic methods will be explored to improve the ECL intensities of other four kinds of CdZnTeS QDs, and the multi-color immunosensors will be constructed to analyze several kinds of biomarkers.

Acknowledgments

This work was supported by the National Key Research and Development Program of China (2017YFA0700404), the National Natural Science Foundation of China (21575022, 21535003, 21375006), the Fundamental Research Funds for the Central Universities (2242016K41055), Qing Lan Project, A Project Funded by the Priority Academic Program Development of Jiangsu Higher Education Institutions (1107047002), and Foundation of Key Laboratory of Sensor Analysis of Tumor Marker, MOE, Qingdao University of Science and Technology (STAM201801).

Appendix A. Supporting Information

Supplementary data associated with this article can be found in the online version at http://dx.doi.org/.

References

Adegoke, O., Park, E.Y., 2016. Sci. Rep. 6, 27288.

Amelia, M., Lincheneau, C., Silvi, S., Credi, A., 2012. Chem. Soc. Rev. 41, 5728-5743.

Bard, A.J., 2004. Electrogenerated Chemiluminescense. Marcel Dekker, New York.

Bell, S.L., Sen, S., 1985. J. Vac. Sci. Technol., A 3, 112-115.

Burke, K.A., Brenckle, M.A., Kaplan, D.L., Omenetto, F.G., 2016. ACS Appl. Mater. Interfaces 8, 16218-16226.

Chang, B.-Y., Chow, K.-F., Crooks, J.A., Mavre, F., Crooks, R.M., 2012. Analyst 137, 2827-2833.

Chikkaveeraiah, B.V., Bhirde, A.A., Morgan, N.Y., Eden, H.S., Chen, X., 2012. ACS

Nano 6, 6546-6561.

Deng, D., Cao, J., Qu, L., Achilefu, S., Gu, Y., 2013a. Phys. Chem. Chem. Phys. 15, 5078-5083.

Deng, D., Qu, L., Achilefu, S., Gu, Y., 2013b. Chem. Commun. 49, 9494-9496.

Ding, S.-J., Liang, S., Nan, F., Liu, X.-L., Wang, J.-H., Zhou, L., Yu, X.-F., Hao, Z.-H., Wang, Q.-Q., 2015. Nanoscale 7, 1970-1976.

Ding, Z., Quinn, B.M., Haram, S.K., Pell, L.E., Korgel, B.A., Bard, A.J., 2002. Science 296, 1293-1297.

Dong, H., Han, T.-T., Ren, L.-L., Ding, S.-N., 2017. J. Electroanal. Chem. 806, 32-40.

Du, D., Zou, Z., Shin, Y., Wang, J., Wu, H., Engelhard, M.H., Liu, J., Aksay, I.A., Lin, Y., 2010. Anal. Chem. 82, 2989-2995.

Feng, T., Qiao, X., Wang, H., Sun, Z., Qi, Y., Hong, C., 2016. J. Mater. Chem. B 4, 990-996.

Ge, J., Yin, Y., 2008. Adv. Mater. 20, 3485-3491.

Han, T.-T., Dong, H., Ren, L.-L., Bao, N., Wu, W.-Z., Ding, S.-N., 2017. Chem. Commun. 53, 5388-5391.

Hu, L., Xu, G., 2010. Chem. Soc. Rev. 39, 3275-3304.

Huang, T., Meng, Q., Jie, G., 2015. Biosens. Bioelectron. 66, 84-88.

Jiang, X., Chai, Y., Wang, H., Yuan, R., 2014. Biosens. Bioelectron. 54, 20-26.

Jing, L., Kershaw, S.V., Kipp, T., Kalytchuk, S., Ding, K., Zeng, J., Jiao, M., Sun, X., Mews, A., Rogach, A.L., Gao, M., 2015. J. Am. Chem. Soc. 137, 2073-2084.

Kalytchuk, S., Zhovtiuk, O., Kershaw, S.V., Zbořil, R., Rogach, A.L., 2016. Small 12, 466-476.

Lai, G., Zhang, H., Yong, J., Yu, A., 2013. Biosens. Bioelectron. 47, 178-183.

Lee, W.I., Bae, Y., Bard, A.J., 2004. J. Am. Chem. Soc. 126, 8358-8359.

Li, H., Yan, J., Ou, W., Liu, H., Liu, S., Wan, Y., 2015b. Biosens. Bioelectron. 64, 111-118.

Li, W., Liu, J., Sun, K., Dou, H., Tao, K., 2010. J. Mater. Chem. 20, 2133-2138.

Li, X., Yu, S., Yan, T., Zhang, Y., Du, B., Wu, D., Wei, Q., 2017. Biosens. Bioelectron. 89, 1020-1025.

Li, Y., Hong, M., Qiu, B., Lin, Z., Chen, Y., Cai, Z., Chen, G., 2014. Biosens. Bioelectron. 54, 358-364.

Li, Z., Wang, Y., Ni, Y., Kokot, S., 2015a. Biosens. Bioelectron. 70, 246-253.

Liu, J., Sun, Z., Deng, Y., Zou, Y., Li, C., Guo, X., Xiong, L., Gao, Y., Li, F., Zhao, D., 2009. Angew. Chem. 121, 5989-5993.

Liu, J.-X., Ding, S.-N., 2016. J. Electroanal. Chem. 781, 395-400.

Liu, R., Zhang, C., Liu, M., 2015. Sens. Actuators, B 216, 255-262.

Liu, S., Zhang, X., Yu, Y., Zou, G., 2014. Biosens. Bioelectron. 55, 203-208.

Liu, X., Jiang, H., Lei, J., Ju, H., 2007. Anal. Chem. 79, 8055-8060.

Myung, N., Bae, Y., Bard, A.J., 2003. Nano Lett. 3, 1053-1055.

Omer, K.M., Bard, A.J., 2009. J. Phys. Chem. C 113, 11575-11578.

Ouyang, J., Fan, F.R.F., Bard, A.J., 1989. J. Electrochem. Soc. 136, 1033-1039.

Qi, H., Zhang, C., 2004. Anal. Chim. Acta 501, 31-35.

Ren, L.-L., Dong, H., Han, T.-T., Chen, Y., Ding, S.-N., 2017. Analyst 142, 3934-3941.

Sahoo, B., Devi, K.S.P., Banerjee, R., Maiti, T.K., Pramanik, P., Dhara, D., 2013. ACS Appl. Mater. Interfaces 5, 3884-3893.

Sung, Y.J., Suk, H.-J., Sung, H.Y., Li, T., Poo, H., Kim, M.-G., 2013. Biosens. Bioelectron. 43, 432-439.

Tang, D., Hou, L., Niessner, R., Xu, M., Gao, Z., Knopp, D., 2013. Biosens. Bioelectron. 46, 37-43.

Wallace, W.L., Bard, A.J., 1979. J. Phys. Chem. 83, 1350-1357.

Wang, S., Harris, E., Shi, J., Chen, A., Parajuli, S., Jing, X., Miao, W., 2010. Phys. Chem. Chem. Phys. 12, 10073-10080.

Wu, M.-S., Liu, Z., Shi, H.-W., Chen, H.-Y., Xu, J.-J., 2015. Anal. Chem. 87, 530-537.

Wu, M.-S., Yuan, D.-J., Xu, J.-J., Chen, H.-Y., 2013. Chem. Sci. 4, 1182-1188.

Wu, P., Zhao, T., Wang, S., Hou, X., 2014. Nanoscale 6, 43-64.

Xing, Y., Chaudry, Q., Shen, C., Kong, K.Y., Zhau, H.E., Chung, L.W., Petros, J.A., O'Regan, R.M., Yezhelyev, M.V., Simons, J.W., Wang, M.D., Nie, S., 2007. Nat.

Protoc. 2, 1152-1165.

Xu, L.-l., Zhang, W., Shang, L., Ma, R.-n., Jia, L.-p., Jia, W.-l., Wang, H.-s., Niu, L., 2017. Biosens. Bioelectron. DOI: 10.1016/j.bios.2017.10.035.

Yang, F., Xu, Z., Wang, J., Zan, F., Dong, C., Ren, J., 2013. Luminescence 28, 392-400.

Yao, J., Li, L., Li, P., Yang, M., 2017. Nanoscale 9, 13364-13383.

Zhang, X., Ding, S.-N., 2016. ACS Sens. 1, 358-365.

Zhang, X., Ding, S.-N., 2017. Sens. Actuators, B 240, 1123-1133.

Zhao, W.-W., Wang, J., Zhu, Y.-C., Xu, J.-J., Chen, H.-Y., 2015a. Anal. Chem. 87, 9520-9531.

Zhao, Y., Zheng, Y., Zhao, C., You, J., Qu, F., 2015b. Biosens. Bioelectron. 71, 200-206.

Zhou, J., Ma, G., Chen, Y., Fang, D., Jiang, D., Chen, H.-y., 2015. Anal. Chem. 87, 8138-8143.

Zhou, X., Zhu, D., Liao, Y., Liu, W., Liu, H., Ma, Z., Xing, D., 2014. Nat. Protoc. 9, 1146–1159.

Highlights

- Quaternary CdZnTeS QDs were used as ECL signal labels.
- The ECL efficiencies of CdZnTeS QDs at cathode and anode were 19.78% and 1.62%.
- The detection of AFP and CA125 were accomplished with direct ECL image analysis.